Robomorphism

A Nonanthropomorphic Wearable Robot

By Dino Accoto, Fabrizio Sergi, Nevio Luigi Tagliamonte, Giorgio Carpino, Angelo Sudano, and Eugenio Guglielmelli

This article describes a novel wearable robot (WR) intended to assist hip and knee flexion/extension through series elastic actuators (SEAs). A nonanthropomorphic (NA) design was pursued to improve ergonomics while optimizing dynamic properties through a smart distribution of swinging masses. Once the anthropomorphism constraint is relaxed, the number of possible architectures becomes very high, and a methodology must be defined to point out the best options. To this purpose, a design methodology, which includes a novel approach to kinematic synthesis, topology selection, and morphological optimization, is also presented. The advantages offered by the novel architecture are demonstrated both theoretically and experimentally. In particular, the results show a low reflected inertia on the user's body, a high backdrivability, and an intrinsic tolerance to misalignments. Such advantages make the proposed robot a promising platform for the development of assistive and rehabilitation systems.

© ISTOCKPHOTO.COM/BESTDESIGNS

Lower-Limb Robots

WRs can replace the functions of a missing limb (robotic prostheses) or provide physical assistance to human movements by acting in parallel to the body (active orthoses). Examples of lower limb portable active orthoses for gait restoration include the Ekso (Ekso Bionics, Berkeley, California), the ReWalk (Argo Medical Technologies, Yokneam Illit, Israel), the REX (REX Bionics, Auckland, New Zealand), the HAL-5 (Cyberdyne, Tsukuba, Japan), and the Vanderbilt Powered Orthosis [1]. Gait assistance can also be provided by treadmill-based robots, which are mainly used in rehabilitation. Examples include the Lokomat (Hocoma, Volketswil, Switzerland), the lower extremity-powered exoskeleton [4], the AutoAmbulator (HealthSouth Co., Birmingham, Alabama), the Active Leg Exoskeleton [5], and the pelvic assist manipulator pneumatically operated gait orthosis [6].

An important objective in the design of an active orthosis is the ergonomics of force transfer. Most of the active orthoses presented so far have anthropomorphic (A) structures with multiple contacts with the human body segments (as opposed to single end-effector robots). This elegant and simple design choice may present some ergonomic drawbacks, as discussed in [7], in terms of micro- and macromisalignments. In fact, an A active orthosis can provide selective torque support to a set of human joints if such joints are aligned with the matching degrees of freedom (DOFs) of the robot. Due to intersubject anthropometric variability, modeling approximations, and slippage of robot fixations over the

Digital Object Identifier 10.1109/MRA.2014.2360276
Date of publication: 19 December 2014

body during motion, a perfect alignment can hardly be achieved. This generates unwanted shear forces on the human skin. To cope with this issue, in [7], special joints are described that are capable of decoupling rotations from translations at the cost of increased inertia and mass, a cost that can be too high in the case of portable robots.

The advantages offered by the novel architecture are demonstrated both theoretically and experimentally.

Conversely, NA architectures can be inherently robust against alignment errors. In addition, the increased design freedom resulting from the relaxation of the anthropomorphism constraint offers the appealing opportunity of optimizing the intrinsic dynamics of the robot, e.g., through a proper distribution of masses.

The optimization of robot dynamics is another important target in impedance-controlled active orthoses because, at frequencies beyond the controller bandwidth, human–robot (HR) interaction becomes strongly affected by the intrinsic dynamics of the robot. Considering the needs of assisting distal joints (i.e., the knee and ankle), mechanical impedance reflected on the user body can become significant.

In this article, we present the design of a lower-extremity NA robot (LENAR), a 4-DOF active orthosis that assists hip and knee flexion/extension during level-ground walking. Using a novel design methodology, the LENAR was conceived and optimized in terms of dynamics (backdrivability) and ergonomics (tolerance to misalignments). The design approach is validated through simulations and experimental tests demonstrating the intrinsic backdrivability and robustness against misalignments.

Design

The synthesis of WR structures, which are not A a priori, is a problem with a bewilderingly high number of potential solutions. Consequently, the problem of selecting a good solution (possibly the optimal) is not amenable to be tackled using an insight-driven engineering approach unless the dimensionality of the design space is first adequately reduced. The primitive stage of defining the topology of a mechanism, i.e., the number of links and their interconnections, is well known in mechanical design as *type synthesis*. We addressed this problem for the synthesis of WRs starting from the following assumptions.

- The parallel structure, comprising human segments and robot links, must be able to support and measure independent hip and knee rotations (i.e., 2 DOFs).
- We constrain our search to planar structures confined in the sagittal plane.
- Only solutions with revolute joints are considered.
- The robot interacts with the subject through pure forces applied to fixations. An ideal HR interaction requires the transfer of forces in the direction orthogonal to the body segments.

The developed methodology extends the methods for manipulator type synthesis to include checks on the kinematic compatibility of WRs through the HR-degeneracy test [9]. This methodology enabled the exhaustive enumeration of

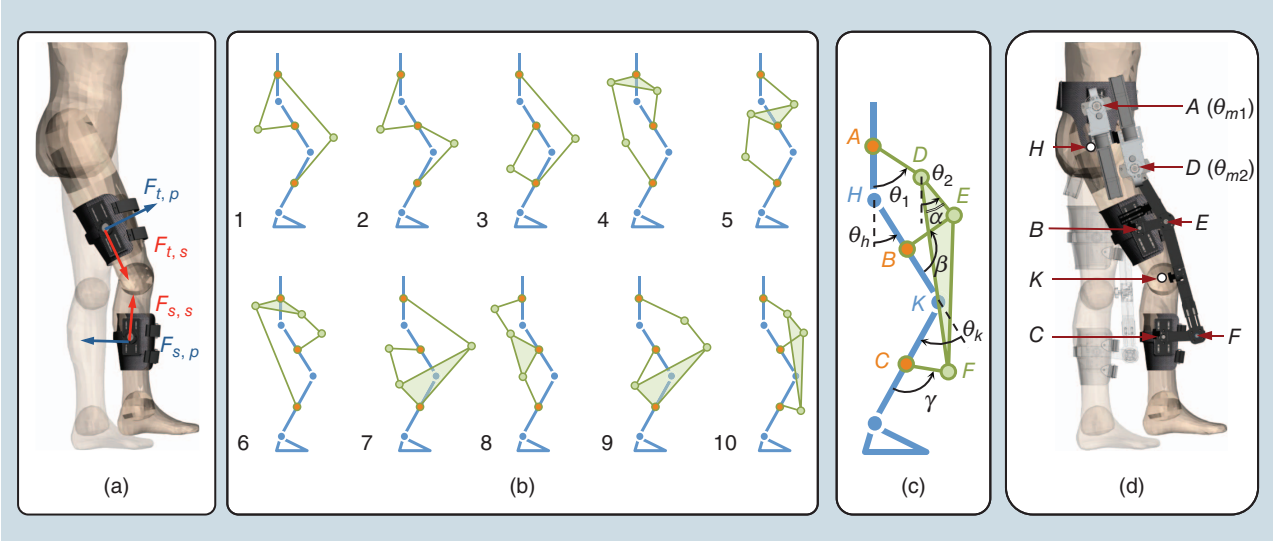

Figure 1. The different stages of the pursued design process, from problem definition, to mechanisms enumeration, to design optimization and detailed mechanical design. (a) Interaction of forces between human segments and WRs. For gait assistance in the sagittal plane, the desired forces F_p are perpendicular to the addressed limbs axes, while shear forces F_s are undesired. (b) An arbitrary morphological representation of the ten generalized solutions for the design problem. The human segments and articulations are shown in blue. The robot joints are shown in orange (on the attachment sites) and green. (c) The kinematic scheme of the mechanism used for morphology optimization that includes both human segments (blue lines) and robot links (green lines). (d) The blank circles, points *H* and *K*, represent the human hip and knee joints, respectively. Points *A* and *D* are the actuated robotic joints, also indicated as m_1 and m_2. The actuator rotations are $\theta_{m_1} = \theta_1$ and $\theta_{m_2} = \theta_2 - \theta_1$. Points *B*, *C*, *E*, and *F* are robot passive revolute joints.

the independent topologies of lower-limb WRs satisfying the previously listed assumptions. There are only ten such topologies, and they are shown in Figure 1(b).

The ten topologies are equivalent from a mobility standpoint. Therefore, a final choice can be made considering ergonomics. We adopted a filtering criterion based on a simple ergonomics principle: a correct interaction requires forces to be applied perpendicularly to the human body segments since tangential forces (shear forces), besides being ineffective for motion generation, may cause discomfort or even tissue damage. It is highly desirable that proper interaction forces are intrinsically generated by the robot because of its mechanical structure. If a human segment is connected to the robot through a binary passive link (i.e., a link connected to the rest of the mechanism through two unactuated revolute joints with parallel rotation axes), static forces are perpendicular to both axes and no torque can be transmitted. If such a link remains orthogonal to the human segment to which it is connected during robot motion, then the ergonomics goal is achieved. This condition is identified in this article as the binary passive link criterion.

This simple principle, once adopted as a design criterion, provides both a way to select a proper topology, among the ten pointed out so far [Figure 1(b)], and an objective in the definition of the specific morphology (i.e., the links length), which must be optimized so that each angle between the connecting passive links and the longitudinal direction of the corresponding human segment [γ and β in Figure 1(c)] is as close as possible to 90° during walking.

Only three topologies (4, 6, and 10) allow for the application of the binary passive link criterion. Among the three, topology 10 was selected because 1) it does not require excessively long links and 2) it allows actuators to be placed proximally, i.e., close to the torso, thus reducing the inertia resulting from the oscillating masses. Analyzing topology 10 in more detail, we notice that the satisfaction of the binary passive link criterion requires the actuators to be placed in *A* and *D* so that links *CF* and *BE* can be passive.

Focusing on topology 10, the set of all possible values of the links' length (*AD, DE, DF, CF,* and *BE*), angle α, and positions of fixation points *A, B,* and *C* represents the search space for the optimal morphology. The search was performed using a scalar fitness function that considers some design objectives, in part already introduced in our preliminary work [10].

Using hip and knee angles (θ_h and θ_k) and torques (τ_h and τ_k) obtained from a standard walking data set [11] (walking speed: 1.3 m/s), we calculated, for every set of morphological parameters, the actuator torques (τ_{m1} and τ_{m2}) and the interaction forces at the fixation points *A* (torso), *B* (thigh), and *C* (shank). The interaction forces at the contact points *B* and *C* were decoupled into the perpendicular (F_p) and shear (F_s) components. Workspace maximization was introduced as another optimization objective. In particular, the robustness of the design with respect to kinematic singularities was quantified and introduced in the fitness function. To this aim, passive joints' angle values were individually checked throughout the planar robot workspace. A singularity checking algorithm was implemented to evaluate whether the angle of passive joints fell below a threshold that was set to 30°. In that case, the otherwise null binary variable *sing* (θ_h, θ_k) was set to one. In the fitness function, the singularity measure was obtained by a two-dimensional summation of sing (θ_h, θ_k), weighted by a function ω_i that accounts for the distance between the given posture and the closest point in the nominal gait cycle (GC) trajectory.

To account for these objectives, the following scalar objective functions for the torque (f_τ), force (f_F), and singularity (f_s) were introduced:

$$
\begin{aligned}
f_\tau &= \max\left[\tau_{m_1}(t), \tau_{m_2}(t)\right]/\tau_{\max} \\
f_F &= \max\left[F_{t,s}(t), F_{s,s}(t)\right]/F_{\max} \\
f_s &= \sum_i \sum_j \operatorname{sing}(\theta_{h,i}, \theta_{k,j}) \cdot w_s(\theta_{h,i}, \theta_{k,j}),
\end{aligned} \tag{1}
$$

having defined the normalization values $\tau_{\max} = 50$ Nm and $F_{\max} = 30$ N. The scalar fitness function is obtained as the algebraic sum of the normalized objectives in (1). The second objective function (f_F) aims at minimizing shear forces. This corresponds to searching the morphology in which, more than in the others, passive binary links stay orthogonal to the human segments to which they are connected.

A hybrid optimization strategy was employed to explore the resulting nine-dimensional space. The body segment lengths retrieved from an anthropometric data set for a 50th percentile man were used. The optimization algorithm consisted of the consecutive application of a genetic algorithm (GA) (implemented through the optimization toolbox of MATLAB R2011b, Mathworks; the GA parameters were population size: 40, max generations: 100, scattered crossover with fraction 0.8, elite count: 2, migration fraction: 0.4, migration interval: 5, stall generation limit: 15, and function tolerance: 10^5) and a deterministic constrained nonlinear optimization (CNLO) method (the active-set algorithm was used; maximum number of iterations: 100; parameters termination tolerance: 10^9). The GA was employed for the preliminary explorative part of the optimization, while CNLO was used for a local refinement, using as an initial guess the best individual produced by the GA. The optimized torque and force profiles are shown in Figure 2.

In addition, passive series elasticity allows impact tolerance and rejection of disturbances due to cyclic foot strike events, reduction of stiction, friction, backlash, and energy buffering.

The optimized morphology requires a peak actuator torque (52 Nm for level-ground walking of an 80-kg mass subject) very close to the peak of the hip and knee torques, calculated via inverse kinematics (48 Nm). Furthermore, the

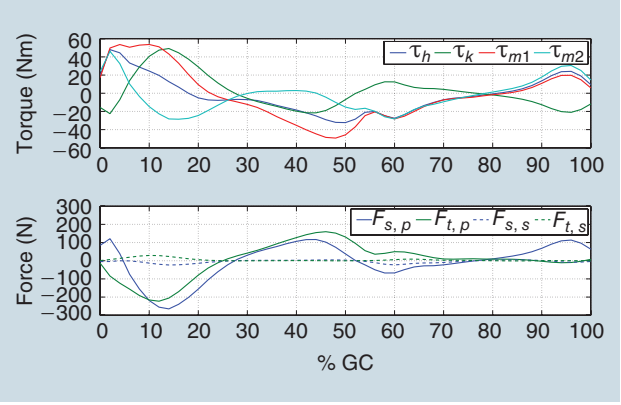

Figure 2. The profiles of the actuator torques and forces at the attachment points *B* (thigh, $F_{t,p}$, and $F_{t,s}$) and *C* (shank, $F_{s,p}$, and $F_{s,s}$) for the optimized solution. The values refer to the level-ground walking of a subject with a mass of 80 kg. Walking speed: 1.4 m/s.

maximum shear force transferred to the supported body segments is 29 N, i.e., only 13% of the peak perpendicular forces. The singularity-free workspace corresponds to the set $\theta_h \in (-20^\circ, 45^\circ)$ $\theta_k \in (0^\circ, 65^\circ)$ and fully contains hip and knee angles obtained during normal walking. For other daily life activities (e.g., ascending/descending stairs and squatting), a different optimization process would be required. Nonetheless, the range of motion allowed by the robot corresponds to 100% of the mean physiological values [12] for hip extension, 38% of hip flexion, and 45% of knee flexion.

The LENAR was conceived and optimized in terms of dynamics (backdrivability) and ergonomics (tolerance to misalignments).

A schematic diagram of the resulting mechanism is shown in Figure 1(d). The optimized solution was fabricated and integrated with custom designed actuators, as detailed in the "Actuators and Control" section.

Prototype Development

Actuators and Control

Custom rotary SEAs were purposively designed. The actuators include a hypoid gear transmission that enables shifting the actuator center of mass with respect to the actuated joint, resulting in the gear motor being placed alongside human limbs [13]. Through the compliant element, the gear motor reflected inertia can be decoupled from the load and used to implement an accurate torque control using the elastic element as a torque sensor. In addition, passive series elasticity allows impact tolerance and rejection of disturbances due to cyclic foot strike events; reduction of stiction, friction, and backlash; and energy buffering. In each SEA [shown in Figure 3(a)], a Maxon EC-4-pole brushless dc motor (rated power: 300 W) is

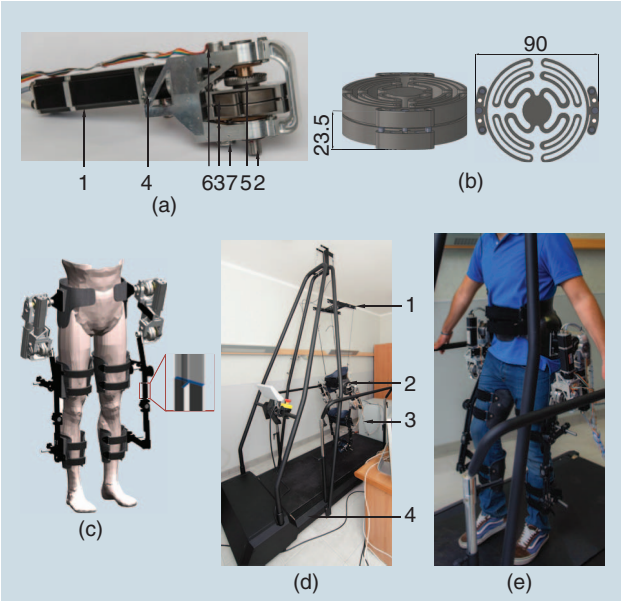

Figure 3. (a) The rotary SEA. 1: DC motor. 2: Output shaft. 3: Torsion spring. 4: Planetary gear box. 5: Hypoid gear. 6 and 7: Absolute encoders. (b) The 3-D CAD drawing of the torsion spring. (c) The 3-D CAD drawing of the LENAR with a detail of the links' T-shaped cross section. (d) The treadmill-based platform. 1: Robot weight support system. 2: WR. 3: Electronic rack. 4: Treadmill. (e) The LENAR worn by a subject.

connected to the output shaft through a monolithic disc-shaped torsion spring [Figure 3(b)]. The spring design was based on an iterative finite-element method simulation-based design and optimization process [14]. Experimental characterization confirmed the predicted torsional stiffness of the spring (k_s = 270.2 Nm/rad). A double reduction stage (comprising a planetary gear box and a hypoid gear with an overall reduction ratio of 64.5:1 and an efficiency of 76.5%) is placed between the motor and the elastic element. The spring deflection is measured using two Gurley A10 absolute encoders (resolution: 1.9×10^{-4} rad). The actuators provide a maximum continuous torque of 30 Nm and a peak torque of 60 Nm.

The SEAs are torque controlled through the measurement of the spring deflection. The control scheme is based on the cascaded approach proposed in [15]. It consists of a proportional-integral (PI) velocity control loop nested in a PI torque control loop. The robot is stiffness controlled in its joint space [the space defined by the actuator rotations $(\theta_{m_1}, \theta_{m_2})$], i.e., the desired torque for each actuated joint (right leg r and left leg l) is set as

$$\tau_{m_i,d}(t) = -k_{m_i}[\theta_{m_i}(t) - \theta_{m_i,d}(t)], \quad (2)$$

where θ_{m_i} and $\theta_{m_i,d}$ are the actual and the desired actuator rotations, respectively, and k_{m_i} is the virtual stiffness $(i = 1,2)$.

The control hardware consists of: 1) four Maxon EPOS2 70/10 control units to drive SEA brushless dc motors, connected to two Maxon shunt regulators DSR 70/30 limiting supply voltage increases and 2) A National Instruments

compactRIO-9022 unit (cRIO), with a reconfigurable field-programmable gate array (FPGA) module and an embedded controller running LabVIEW real-time (RT) software. The cRIO also comprises two high-speed digital input/ouput modules (NI 9403) as interfaces with robot encoders, and a high-speed (1-Mbit/s) controller area network (CAN) module (NI 9853) for communication with the EPOS2 units. The FPGA module acquires SEA absolute encoder signals (synchronous serial interface communication, 10 kHz), runs torque controllers (1 kHz), and executes CAN bus low-level communication with the EPOS2 units (transmission of motor commands and reading of current, position, and velocity). Torque controllers generate the desired velocity set points that are transmitted via a CANopen protocol to the velocity controllers running on the EPOS2 devices (1 kHz). The high-level stiffness controller runs on the cRIO RT level at 200 Hz. Feedback for torque and stiffness controllers is based on the measurement of the absolute encoders, filtered using second-order low-pass Butterworth filters, with a cutoff frequency of 40 Hz. All of the control components and power supplies are located in a remote rack.

The torque control bandwidth of the actuator in blocked output conditions is 6.5 Hz [13]. The stiffness control performance was evaluated with the actuator commanded to generate elastic torques with different values of the virtual stiffness k_m, while keeping $\theta_{m,d}$ fixed. In these conditions, the output shaft was manually perturbed with oscillatory movements (amplitude of about 80°). Tests were carried out varying k_m in the range $[0.1\,k_s, k_s]$, with steps of $0.1\,k_s$. The estimated mechanical impedance transfer function $\hat{Z}(f)$, calculated using a nonparametric identification method [13], is reported in Figure 4. Data are shown in the range 0.6–6 Hz, where the coherence between the imposed velocity and the interaction torque was found to be greater than 0.8 for all of the tests. The performance degradation in rendering a virtual stiffness much lower than the physical one (k_s) is in line with the literature results [19].

As expected from the theoretical studies [20], the system becomes not passive [phase of $\hat{Z}(f)$ smaller than $-90°$] for $k_m > 0.6k_s$. Since passivity is a conservative condition for coupled stability, no stability issues were experienced during interaction tests with manual perturbations.

To estimate the order of magnitude of torques needed by the robot to move itself (i.e., in free space, compensating for gravitational and frictional effects), physiological walking movements were produced with the robot suspended to the frame and with the actuator's stiffness controlled. With reference to Figure 1(c), starting from hip and knee desired rotations $\theta_{h,d}$ and $\theta_{k,d}$, it was possible to derive, based on inverse kinematics calculations, the actuator rotations $\theta_{m_{1,d}}$ and $\theta_{m_{2,d}}$ to be used in the stiffness control (2) and needed to produce the desired kinematic patterns in the human joint space. The data on hip and knee physiological patterns ($\theta_{h,d}$ and $\theta_{k,d}$) in the sagittal plane for healthy young subjects were retrieved from [11]. These data were adapted to a slow-walking GC duration (3.2 s), and the angles' amplitude was scaled by a factor of 1.4. The same profile was used for both legs, with a phase shift of π. The virtual stiffness was set to $k_{m_{il}} = k_{m_{ir}} = 0.2k_s$ for $i = 1, 2$. The results (Figure 5) show that the system can produce the desired walking patterns with peak actuation torques lower than 7 Nm, i.e., 12% of the maximum value allowed by the actuators. Therefore, 88% of the actuator deliverable torque is still available to provide physical

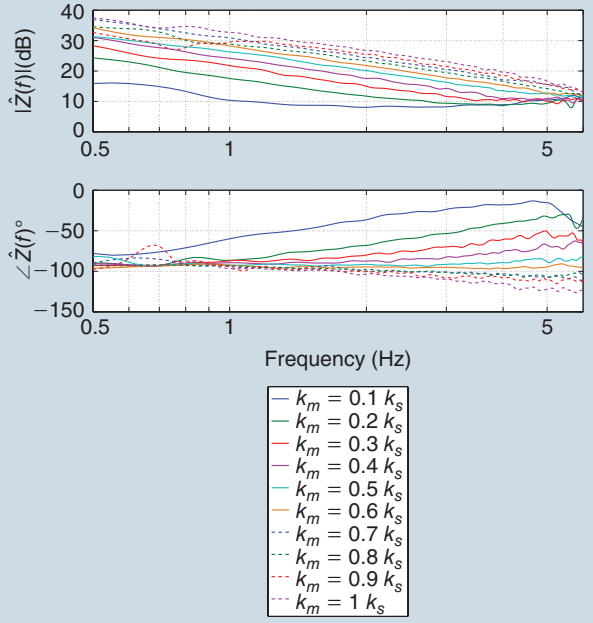

Figure 4. A Bode plot of the SEA transfer function $\hat{Z}(f)$ when rendering a pure elastic behavior with different virtual stiffness values k_m. For $k_m > 0.6k_s$, the system becomes not passive (dashed lines), as expected from the theoretical studies [20].

Table 1. The prototype performance.

Quantity	Measure	Unit
SEAs		
Maximum continuous torque	30	Nm
Peak torque	60	Nm
Maximum continuous speed	5.8	rad/s
Rated power	300	W
Intrinsic stiffness	270.2	Nm/rad
Torque control bandwidth (30 Nm ptp)	6.5	Hz
Robot		
Hip maximum back driving torques	10	Nm
Knee maximum back driving torques	5	Nm
Hip range of motion	45 (flex)–20 (ext)	°
Knee range of motion	65 (flex)–0 (ext)	°
Maximum walking speed	5	km/h
User height	1.65–1.85	m

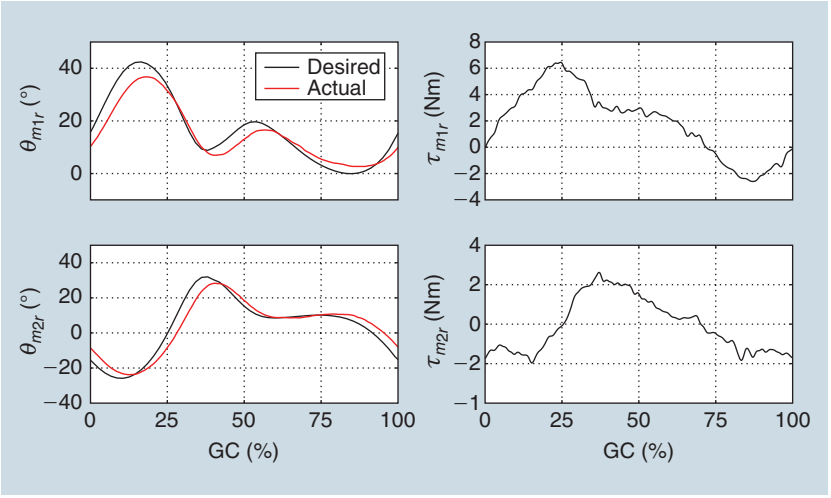

Figure 5. The tests when moving the robot (right leg) in the free space. The desired positions for the stiffness controller were offline calculated from the inverse kinematics problem to achieve physiological gait in the human joints space (data adapted from [11]).

assistance during walking and to compensate for dynamical effects. A summary of the limit performance of the developed prototype is reported in Table 1.

Wearing and Usage

With reference to Figure 1(d), the LENAR comprises a pelvis cuff (hosting joint *A*) and, for each leg, two SEAs actuating joints *A* and *D*, one thigh cuff (hosting joint *B*), and one shank cuff (hosting joint *C*). The segment *EF* can be adjusted to accommodate users between the fifth and 95th percentile of the adult population (see Table 1). The sliders allow for the regulation of the position of joints *A*, *B*, and *C*. To reduce the parasitic compliance due to links' flexion–torsion, the links were built from class 7075 aluminum alloy (Ergal) using a T-shaped cross section. In addition, the carbon fiber cuffs embed an aluminum insert for increased stiffness. An overview of the WR is shown in Figure 3(c).

As shown in Figure 3(d), the robot is suspended over a treadmill (an N-Mill, ForceLink B.V with a walking surface of 70×175 cm^2) through a passive vacuum cylinder, which provides an upward constant force equal to the weight of the robot (about 25 kg), without introducing serial elasticity and possible resonances. The height of the support can be manually adjusted to accommodate users with different anthropometric measures. Cables are used to connect the weight support system to the pelvis cuff. This allows passive pelvis rotations. Hip adduction/abduction motion is also allowed by the compliance of the carbon fiber pelvis cuff. Intra/extra rotation, which is not necessary for walking on a treadmill, is constrained.

When the user accesses the platform, the pelvis cuff is adjusted to a comfortable position. Then, the suspension height is regulated by manually acting on the weight balancing system. Subsequently, Velcro straps on the pelvis cuff are fastened. Then, the thigh and shank cuffs are worn and fastened. The adjustable links and sliders on the cuffs (see the "Wearing and Usage" section) are regulated to allow links *BE* and *CF* [see Figure 1(d)] to be almost perpendicular to the human segments.

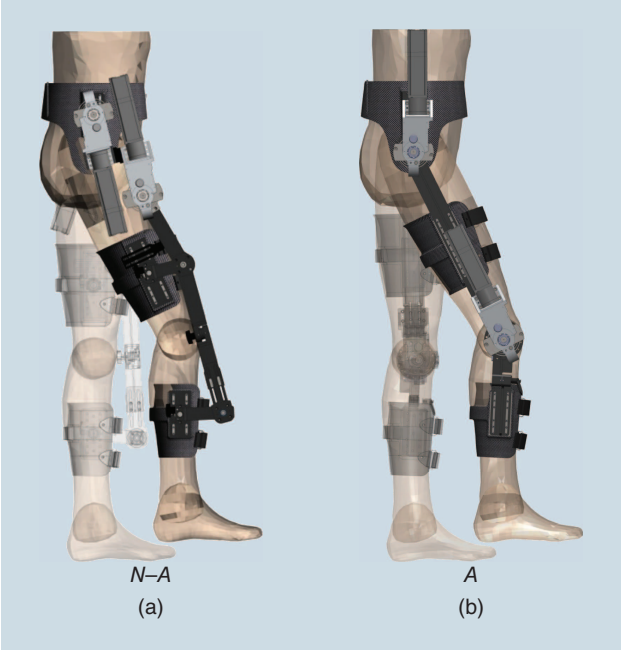

Figure 6. A schematic of the two models considered for the dynamic analysis of the robot. (a) The NA robot (LENAR). (b) The A robot using the same actuators of the LENAR.

Advantages of Nonanthropomorphism

Dynamic Analysis

A dynamic analysis based on the generalized inertia ellipsoid [18] in the human joint space (θ_h, θ_k) during normal walking [11] helps assess the potential benefits introduced by the NA design. The dynamics of an n-DOF robotic system can be written as

$$M(q)\ddot{q} + C(q,\dot{q})\dot{q} + g(q) = \tau, \tag{3}$$

where q is the $n \times 1$ vector of the generalized coordinates, $M(q)$ is the $n \times n$ inertia matrix, $C(q,\dot{q})$ is the $n \times n$ matrix representing Coriolis/centrifugal terms, $g(q)$ is the $n \times 1$ gravity vector, and τ is the $n \times 1$ vector of the actuation forces/torques applied on the generalized coordinates.

We compared the equivalent inertia reflected at the hip and knee joints by the NA robot, with the one calculated in two conditions: 1) the no-robot (N-R) condition, in which only the intrinsic inertia of the legs is reflected on the hip and knee joints and 2) the A robot condition, in which the same actuators described in the "Actuators and Control" section are used

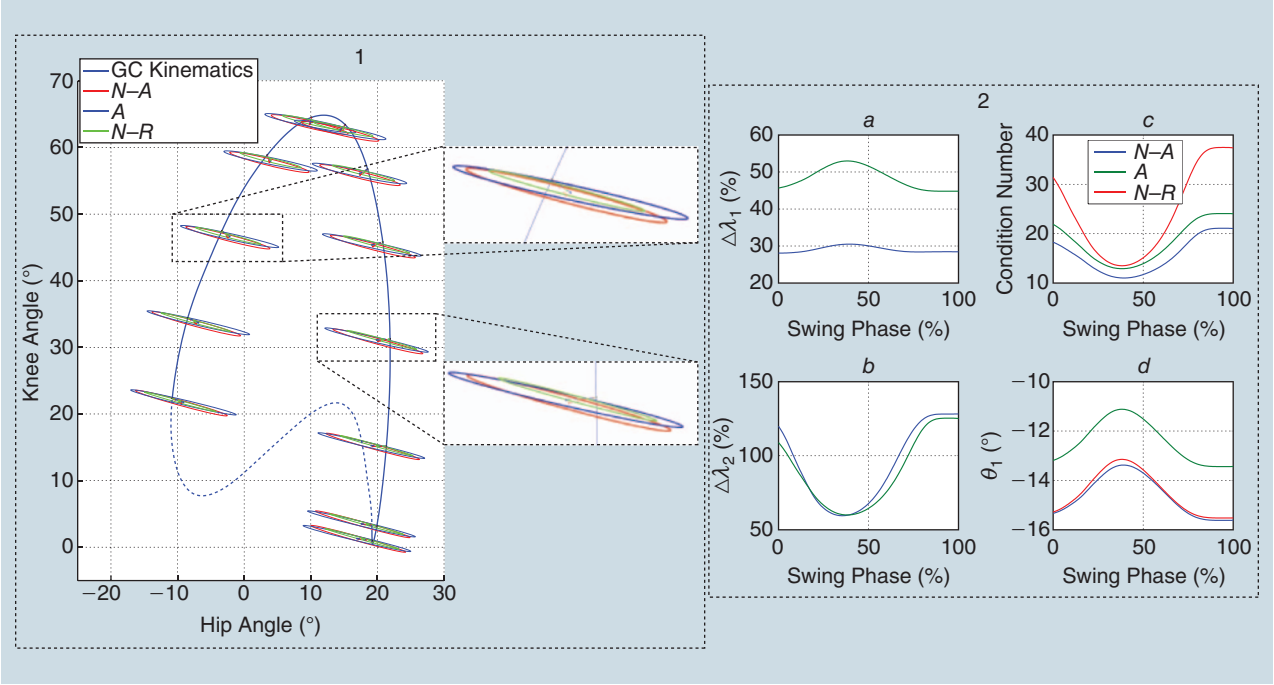

Figure 7. 1) A comparison of the resulting inertia for the NA design described in this article, the equivalent A system, and the N-R condition, as determined by the equivalent inertia ellipses in the human joint space during the swing phase (the continuous line in the GC depicted). A standard gait pattern moves clockwise along the blue line. 2) The ratio between a) the maximum and b) the minimum eigenvalue of the inertia matrix for the NA and A systems and the correspondent eigenvalue of the N-R condition, in the same posture. c) The condition number throughout the stance phase. d) The measure of rotation of the principal axis of inertia, relative to the N-R case, for both the NA condition and the A condition throughout the swing phase.

in an A architecture. To simplify the comparison, in both A and NA cases, the actuators are assumed to be directly connected to the corresponding actuated joints (Figure 6), although actuator remotization could improve the dynamic performance of both architectures. In this analysis, we consider the torso grounded, and we focus on the swing since it is the phase mostly dominated by inertia.

To make the comparison conservative (i.e., slightly biased in favor of the A architecture), we introduced further assumptions on the A structure: 1) the stator of the hip actuator is framed to the torso so that only its rotor contributes to the inertia reflected at the hip and gravitational effects are minimized, 2) as shown in Figure 6(b), the knee actuator is placed so that its center of mass is as proximal as possible (to minimize the associated swinging mass), and 3) the links are massless.

The impedance perceived by a user can be quantified by the inertia matrix alone since full inverse dynamics simulations, considering both human segments and robotic links, evidenced that the peak and RMS values of the torques calculated for the $C(q,\dot{q})$ matrix are much lower than inertial torques for the NA, N-R, and A conditions. For instance, the peak Coriolis contribution is 7% of the peak inertial torque for the hip joint and 20% for the knee joint.

The mass needed to support a distal joint (in our case, the knee joint) obviously increases the inertial load on the proximal joint (in our case, the hip joint) (Figure 7). However, the NA design reduces such an increase compared with the A

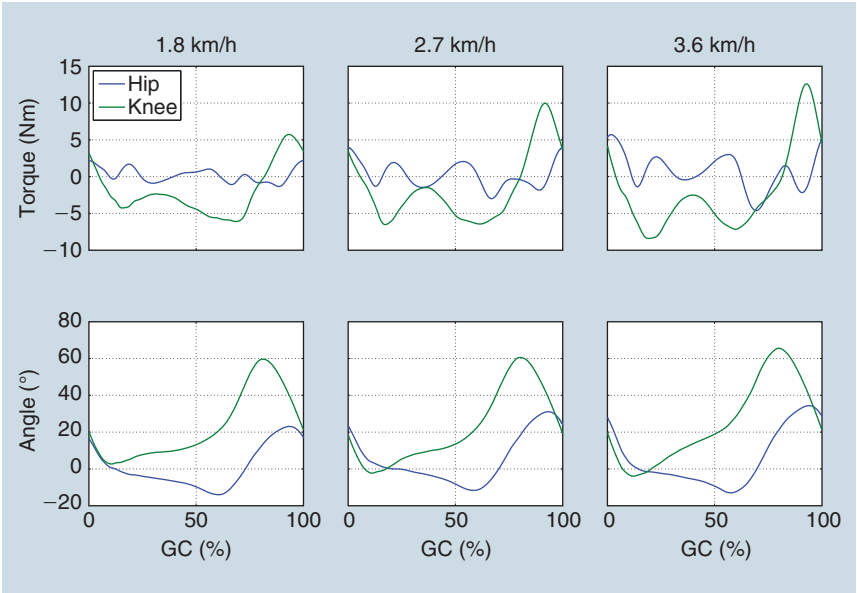

Figure 8. The HR interaction torques in the human joint space (as a function of the percentage of the GC) and joint rotations for the backdrivability tests performed at different walking speeds. The data are averaged over 30 s for each trial.

Table 2. The dynamical comparison of the NA robot (λ_i are in kg m^2, and θ_1 is in °).

	N-A	A	N-R
λ_1 - Mean	3.33	3.83	2.5
λ_1 - STD	0.26	0.25	0.21
$\Delta\lambda_1$ - Mean	29	48	–
$\Delta\lambda_1$ - STD	0.8	3	–
λ_2 - Mean	0.22	0.21	0.12
λ_2 - STD	0.03	0.03	0.03
$\Delta\lambda_2$ - Mean	92.4	88.1	–
$\Delta\lambda_2$ - STD	25.76	23.6	–
$\kappa(M)$ - Mean	15.4	18.1	23.8
$\kappa(M)$ - STD	3.6	4	8.7
θ_1 - Mean	−14.6	−12.4	−14.5
θ_1 - STD	0.8	0.8	0.8

case. The inertia (λ_1) perceived when moving in the principal direction is calculated as the square root of the maximum eigenvalue of the quadratic form $M^T(q)M(q)$.

To quantify the effect of the robot design on the resulting inertia, we considered the measures shown in Figure 7. The first two measures are the percent increase of λ_i, for both the NA and A robots, compared with the value of λ_i calculated for each posture in the N-R condition

$$\Delta\lambda_i^j(t) = 100\frac{\lambda_i^j(q(t))}{\lambda_i^{N-R}(q(t))}, \quad i = 1,2. \tag{4}$$

The subscript i refers to either the maximum (for $i = 1$) or to the minimum (for $i = 2$) eigenvalue of the inertia matrix quadratic form, whereas the subscript j refers to the N-A condition and the A condition. Furthermore, we define the condition number $[\kappa(M)]$ of the inertia matrix as a measure of inertial anisotropy in each considered posture of the swing phase. The condition number is the ratio between the maximum and minimum inertia matrix eigenvalues. Finally, we quantify the rotation of the principal axis (θ_1^j) by measuring the angle between the principal vector $v_1^j\,(j = N-R, A)$ and the $\hat{\theta}_h$ unit vector as $\theta_1^j = \text{acos}(v_i^j \cdot \hat{\theta}_h)$.

A higher value of θ_1^j results in a larger angle between the principal axis of inertia v_1 and the hip angle coordinate axis $\hat{\theta}_h$, which implies a reduction of the equivalent inertia displayed at the hip joint (keeping the shape of the ellipse constant).

We summarized in Table 2 the mean and standard deviation (STD) of the four measures of interest during the swing phase, as well as the absolute values corresponding to the N-R condition. The analysis of the average resulting inertia of the NA robot shows a 29% increase of the maximum principal value, compared with the N-R condition, while the lowest principal value increases by 93%. The unavoidable increase of perceived inertia, due to the need for oscillating masses to support the distal joint, is lower than the increase in inertia in the A design. In particular, the increase of the lowest principal value is substantially the same in the NA and A cases, while the increase in the principal eigenvalue is higher in the A case (48 versus 29%). The parameter chosen to represent the orientation of the inertia ellipse θ_1^j is related to the relative contribution of inertia perceived at the hip joint compared with the inertia perceived at the knee joint; its analysis shows that the NA design minimally perturbs the orientation of the inertia ellipse compared with the N-R condition. Instead, the A design results in an ellipse with a more horizontal principal axis, reflecting the disproportionate relative increase in the inertia perceived at the hip joint compared with the one reflected to the knee joint.

The condition number in the NA is 15.4, compared with 18.1 of the A solution, indicating that the inertia perceived by the user is more isotropic in the two axes. The N-R solution has an even higher degree of anisotropy of the displayed inertia (23.8); this is due to the fact that the minimum eigenvalue λ_2 is only equal to 0.12 kg m^2, and the necessity of supporting the distal joints unavoidably increases this value, hence increasing the condition number.

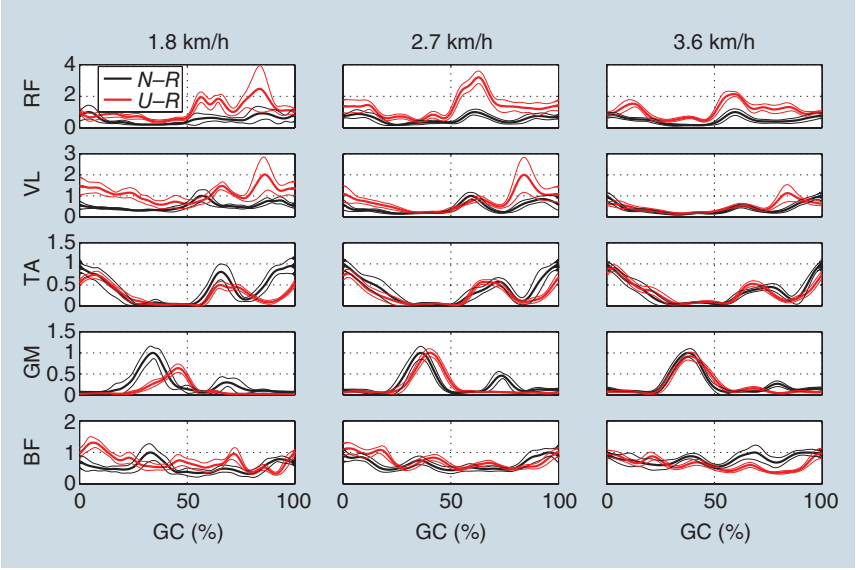

Figure 9. The EMG activity of RF, VL, TA, GM, and BF for the tests at three different speeds with the subject during free walking (N-R) and wearing the U-R. The thin lines represent the standard deviation (STD).

Backdrivability

Backdrivability was assessed through experimental tests aimed at evaluating the muscular activity and torques needed to backdrive the robot while walking at different speeds (1.8, 2.7,

and 3.6 km/h). Before the tests, the subject (male, 24 years of age, height 178 cm, and body mass 90 kg) was asked to walk freely at a self-selected cadence for 10 min to get familiar with the device and the testing environment. A photo of the subject wearing the robot is shown in Figure 3(e). Triaxis accelerometers (DE-ACCM3D, Dimension Engineering), whose signals were acquired through an NI 9205 analog input module, were placed on the heels of the subject's shoes to detect the foot's contact with the ground. The subject was first asked to walk at different walking speeds without the robot (N-R), to set the baseline, and then wearing the robot with the actuators switched off [unpowered robot (UR)]. Surface EMG electrodes (DENIS 5026, Spes Medica) connected to two four-channel amplifiers (QP522, Grass Technologies) were used to measure muscular activity. The activity of the five muscles on the right leg was measured: 1) the rectus femoris, 2) the vastus lateralis, 3) the tibialis anterior, 4) the gastrocnemius medialis, and 5) the biceps femoris. The signals were band pass filtered (10−1,000 Hz) and acquired with the cRIO control unit through the NI 9205 module (sampling frequency: 2 kHz). During post processing, the signals were full-wave rectified and low-pass filtered using a zero-lag second-order Butterworth filter with a cutoff frequency of 5 Hz for smoothing. The data were segmented based on heel contact events, averaged over 30 s of the trial, and normalized with respect to the peak value of the EMG activity (for each muscle and for each walking speed) of the N-R tests.

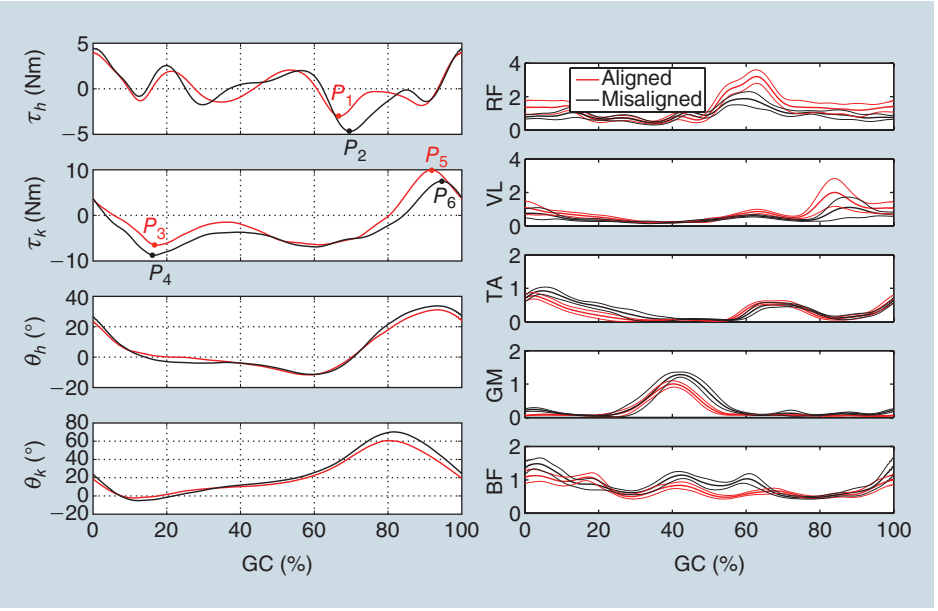

Figure 10. A comparison between the torques, angles, and EMG activity during tests with the robot optimally mounted on the subject and with the introduction of mounting errors at a self-selected walking speed of 2.7 km/h. The thin lines indicate the STD. The maximum peak torque increases at the hip and knee joints, respectively, are 56% (between P_1 and P_2) and 34% (between P_3 and P_4). The peak torque at the knee decreases by 25% between points P_5 and P_6.

Table 3. The calibration parameters.

Link/Segment	BK	DF	KC	EF
	Robot aligned			
Length (mm)	150	560	240	370
	Robot misaligned			
Length (mm)	140	530	210	340

During the tests, joint rotations ($\theta_{m_{ir}}$ and $\theta_{m_{il}}\, i = 1,2$) and HR interaction torques ($\tau_{m_{ir}}$ and $\tau_{m_{il}}\, i = 1,2$) in the robot joint space were recorded. The angles (θ_h, θ_k) and torques (τ_h, τ_k) of the hip and knee joints were calculated using the transformation from the robot joint space to the human joint space. The actuator and human joint angles, averaged over 30 s in steady-state condition, are reported in Figure 8 for the test at different walking speeds. The mean GC duration for the tests in N-R mode was 1.7, 1.4, and 1.2 s, respectively. In the human joint space, the peak backdriving torques were 6.2, 10.0, and 12.6 Nm for the three selected speeds (knee joint). With unpowered actuators, a subject has to deliver low additional torques to backdrive the robot (in the range of 11–23% of those required during free overground walking). This result quantitatively demonstrates the intrinsic backdrivability of the robot enabled by the reduced inertia reflected on the body and by the low impedance of the actuators.

The reduced perturbation to the human natural motion was also demonstrated by the EMG signals reported in Figure 9, where muscular activities in the U-R and N-R conditions are compared. It can be noticed that the presence of the robot, although unpowered, produces major alterations to natural muscular activation only at low walking speeds. In particular, with respect to the N-R condition, at 1.8 km/h, the RMS activity of the rectus femoris (RF) and of the vastus lateralis (VL) are about doubled, while that of the tibialis anterior (TA) and gastrocnemius medialis (GM) decreases by about 40%, and that of the biceps femoris (BF) increases by about 30%. In

It is highly desirable that proper interaction forces are intrinsically generated by the robot because of its mechanical structure.

addition, the maximum EMG variation occurs at all the walking speeds for the RF and the VL.

Finally, the walking cadence in the U-R condition changed less than 30% at the three different speeds (the recorded GC durations were 1.8, 1.4, and 1.3 s, respectively).

Tolerance to Misalignments

Tolerance to misalignments simplifies both wearing and calibration procedures. To demonstrate this tolerance, which is the second objective pursued with the design methodology, a numerical analysis and experimental tests were performed.

The sensitivity of shear forces during walking to the nonoptimal placement of the fixation points was investigated numerically. We moved points *A*, *B*, and *C* (±5 mm with steps of 2.5 mm) to simulate 125 misalignment conditions. In the worst case, the peak shear forces were about 30 and 18% of the peak perpendicular forces (compared with 13% of the ideal case), for the thigh and the shank attachment points, respectively.

We also complemented the analysis with experimental trials, repeating the tests described in the "Backdrivability" section with the robot calibrated to fit a user about 5 cm shorter than the real tester (see Table 3). The user, who was asked to self-select the walking speed (2.7 km/h), showed a GC duration that did not significantly differ from the case in which the robot was correctly mounted. As shown in Figure 10, the kinematic patterns, human joint delivered torques, and EMG activity were not significantly altered when the robot was misaligned.

The increased design freedom [optional: resulting from the relaxation of the anthropomorphism constraint] offers the appealing opportunity of optimizing the intrinsic dynamics of the robot.

In detail, the RMS variation of the hip torque (τ_h) is 1.1 Nm, while the RMS variation of the knee torque (τ_k) is 2.0 Nm. The RMS variation of hip and knee angles are 2.1° and 5.2°, respectively. The variation of the EMG signals is not statistically significant. Last but not least, no perceivable discomfort was reported.

Conclusions

Because of their simplicity, A architectures are by far the most frequently used in assistive and rehabilitation robotics. Such architectures, mounted in parallel to the human body, require that robot and human joints are accurately aligned, as misalignments would result in kinematic incompatibilities impeding the movement of the limbs or causing physical discomfort. In addition, fixing the topology of the robot reduces the DOFs that the designer can exploit to endow the robot with the desired dynamical features, such as the minimization of swinging masses and the intrinsic control of the direction of the interaction forces.

The LENAR was designed starting from the relaxation of the A constraint. This tremendously enlarges the search space for type synthesis. In this article, we presented a design approach based on: 1) the systematic search of all robot configurations with a desired mobility to provide mechanical support to a given number of human joints, 2) the selection of a candidate design solution, and 3) the design optimization to improve the ergonomics and actuation requirements. Through the novel methodology pursued, it was possible to improve, compared with an equivalent A design, both the dynamical properties, in terms of reflected inertia, and the ergonomics of force transfer, in terms of robustness to wearing misalignments. Such aspects were validated both numerically and experimentally, as summarized next.

As for dynamic improvements, the analysis of the average resulting inertia of the NA robot shows a 29% increase for the maximum principal value, compared with the N-R condition. Such an increase is smaller than the one that would occur in an A design using the same actuators (48%). The increase in the lowest principal value of inertia is high in both robot designs (93% for the NA and 89% for the A) but applies to a direction characterized by a significantly smaller inertial loading (on average, 0.21 kg m^2 compared with 3.3 km m^2 for the proximal joint). To further investigate the dynamical properties, we defined a parameter that indicates the orientation of the displayed inertia ellipse in the human joint space. This parameter describes the relative contribution of the inertia perceived at the hip joint compared with the inertia perceived at the knee joint. Our analysis shows that the NA design minimally perturbs the orientation of the inertia ellipse compared with the N-R condition. Instead, the A design results in an ellipse with a principal axis much more aligned with the hip joint axis, reflecting the disproportionate relative increase in the inertia perceived at the hip joint compared with that reflected to the knee joint. The analysis also demonstrates that the proposed design mitigates the unavoidable increase in equivalent inertia displayed to the human joints. Based on the assumptions of the comparison, it can be concluded that the dynamical advantages are intrinsic to the morphology of the designed NA robot. Indeed, any real A robot (i.e., with links with not null mass) using the same actuation system would exhibit a dynamic performance lower than that of the LENAR. Such a result supports the choice of an NA design in lower-limb active orthoses, given the fact that walking is a dynamical process dominated by inertia.

Another important feature of the proposed design is that it locates the actuators, which are the heaviest swinging masses, close to the torso. Despite the high torque and power of the actuators used (two compliant actuators per leg, each with a peak torque of 60 Nm and a rated power of 300 W), the robot is highly backdrivable even when unpowered, with backdriving torques in the human joint space corresponding to 11–23% of those delivered by human joints during free

overground walking. These results were also confirmed by small alterations in the EMG activity of the five muscles of a single leg when compared with the case where the subject walked without wearing the robot.

As for ergonomics, the possibility to allow fast-wearing procedures is an often overlooked feature of WRs, especially in the rehabilitation scenario, where the maximization of the time devoted to the actual therapy is of prominent importance. Under this regard, the NA structure simplifies the wearing procedure since the robot joints must not be aligned to the human joints. We could estimate that the first wearing procedure with a new subject takes about 15–25 min, while about 5–10 min is enough for successive procedures. Interaction tests, performed with robot link lengths set at different values from the reference ones, demonstrated no significant alterations to the EMG activity and to torque and angle profiles.

The proposed design approach lends itself to the future development of both novel treadmill-based rehabilitation robots (e.g., with remotized actuators) and novel robots with full mobility (e.g., with portable controllers and energy source).

References

[1] R. Farris, H. Quintero, and M. Goldfarb, "Preliminary evaluation of a powered lower limb orthosis to aid walking in paraplegic individuals," *IEEE Trans. Neural Syst. Rehab. Eng.*, vol. 19, no. 6, pp. 652–659, 2011.

[2] P. D. Neuhaus, J. H. Noorden, T. J. Craig, T. Torres, J. Kirschbaum, and J. E. Pratt, "Design and evaluation of Mina: A robotic orthosis for paraplegics," in *Proc. IEEE Int. Conf. Rehabilitation Robotics*, 2011, pp. 1–8.

[3] T. Nakamura, K. Saito, Z. Wang, and K. Kosuge, "Realizing a posture-based wearable antigravity muscles support system for lower extremities," in *Proc. 9th Int. Conf. Rehabilitation Robotics*, 2005, pp. 273–276.

[4] J. Veneman, R. Kruidhof, E. Hekman, R. Ekkelenkamp, E. V. Asseldonk, and H. van der Kooij, "Design and evaluation of the LOPES exoskeleton robot for interactive gait rehabilitation," *IEEE Trans. Neural Syst. Rehab. Eng.*, vol. 15, no. 3, pp. 379–386, 2007.

[5] S. Banala, S. H. Kim, S. Agrawal, and J. Scholz, "Robot assisted gait training with active leg exoskeleton (ALEX)," *IEEE Trans. Neural Syst. Rehab. Eng.*, vol. 17, no. 1, pp. 2–8, 2009.

[6] D. Aoyagi, W. Ichinose, S. Harkema, D. Reinkensmeyer, and J. Bobrow, "A robot and control algorithm that can synchronously assist in naturalistic motion during body-weight-supported gait training following neurologic injury," *IEEE Trans. Neural Syst. Rehab. Eng.*, vol. 15, no. 3, pp. 387–400, 2007.

[7] A. Stienen, E. Hekman, F. van der Helm, and H. van der Kooij, "Self-aligning exoskeleton axes through decoupling of joint rotations and translations," *IEEE Trans. Robot.*, vol. 25, no. 3, pp. 628–633, 2009.

[8] X. Kong and C. Gosselin, *Type Synthesis of Parallel Mechanisms*. vol. 33, Berlin, Germany: Springer-Verlag, 2007.

[9] F. Sergi, D. Accoto, N. L. Tagliamonte, G. Carpino, and E. Guglielmelli, "A systematic graph-based method for the kinematic synthesis of non-anthropomorphic wearable robots for the lower limbs," *Front. Mech. Eng.*, vol. 6, no. 1, pp. 61–70, 2011.

[10] F. Sergi, D. Accoto, N. L. Tagliamonte, G. Carpino, and E. Guglielmelli, "Kinematic synthesis, optimization and analysis of a non-anthropomorphic 2-DOF wearable orthosis for gait assistance," in *Proc. IEEE/RSJ Int. Conf. Intelligent Robots Systems*, 2012, pp. 4303–4308.

[11] D. Winter, *Biomechanics and Motor Control of Human Movement*. Hoboken, NJ: Wiley, 2009.

[12] A. Roaas and G. B. J. Andersson, "Normal range of motion of the hip, knee and ankle joints in male subjects, 30–40 years of age," *Acta Orthop.*, vol. 53, no. 2, pp. 205–208, 1982.

[13] D. Accoto, G. Carpino, F. Sergi, N. L. Tagliamonte, L. Zollo, and E. Guglielmelli, "Design and characterization of a novel high-power series elastic actuator for a lower limb robotic orthosis," *Int. J. Adv. Robot. Syst.*, vol. 10, no. 359, pp. 1–12, 2013.

[14] G. Carpino, D. Accoto, F. Sergi, N. L. Tagliamonte, and E. Guglielmelli, "A novel compact torsional spring for series elastic actuators for assistive wearable robots," *J. Mech. Des.*, vol. 134, no. 12, pp. 121002-1–121002-10, 2012.

[15] H. Vallery, J. Veneman, E. van Asseldonk, R. Ekkelenkamp, M. Buss, and H. van der Kooij, "Compliant actuation of rehabilitation robots: Benefits and limitations of series elastic actuators," *IEEE Robot. Automat. Mag.*, vol. 15, no. 3, pp. 60–69, 2008.

[16] L. W. Tsai, *Robot Analysis and Design: The Mechanics of Serial and Parallel Manipulators*, 1st ed. Hoboken, NJ: John Wiley, 1999.

[17] F. H. Ghorbel, O. Chételat, R. Gunawardana, and R. Longchamp, "Modeling and set point control of closed-chain mechanisms: Theory and experiment," *IEEE Trans. Control Syst. Technol.*, vol. 8, no. 5, pp. 801–815, 2000.

[18] H. Asada, "A geometrical representation of manipulator dynamics and its application to arm design," *J. Dyn. Syst. Meas. Control*, vol. 105, no. 3, pp. 131–142, 1983.

[19] F. Sergi, D. Accoto, G. Carpino, N. Tagliamonte, and E. Guglielmelli, "Design and characterization of a compact rotary series elastic actuator for knee assistance during overground walking," in *Proc. IEEE RAS EMBS Int. Conf. Biomedical Robotics Biomechatronics*, 2012, pp. 1931–1936.

[20] N. L. Tagliamonte and D. Accoto, "Passivity constraints for the impedance control of series elastic actuators," *Proc. Inst. Mech. Eng. Part I: J. Syst. Control Eng.*, vol. 228, no. 3, pp. 138–153, 2014.

Dino Accoto, Università Campus Bio-Medico di Roma, Rome, Italy. E-mail: d.accoto@unicampus.it.

Fabrizio Sergi, Rice University, Houston, Texas, United States. E-mail: fabs@rice.edu.

Nevio Luigi Tagliamonte, Università Campus Bio-Medico di Roma, Rome, Italy. E-mail: n.tagliamonte@unicampus.it.

Giorgio Carpino, Università Campus Bio-Medico di Roma, Rome, Italy. E-mail: g.carpino@unicampus.it.

Angelo Sudano, Università Campus Bio-Medico di Roma, Rome, Italy. E-mail: a.sudano@unicampus.it.

Eugenio Guglielmelli, Università Campus Bio-Medico di Roma, Rome, Italy. E-mail: e.guglielmelli@unicampus.it.